Europe PMC Funders Group
Author Manuscript
ACS Sens. Author manuscript; available in PMC 2021 April 12.

Published in final edited form as:
ACS Sens. 2016 July 18; 1(8): 1028–1035. doi:10.1021/acssensors.6b00272.

Electrical Impedance Spectroscopy for Microtissue Spheroid Analysis in Hanging-Drop Networks

Yannick R. F. Schmid[†,‡], **Sebastian C. Bürgel**[†], **Patrick M. Misun**, **Andreas Hierlemann**, **Olivier Frey**[*]
Department of Biosystems Science and Engineering, Bio Engineering Laboratory, ETH Zurich, Mattenstrasse 26, CH-4058 Basel, Switzerland

Abstract

Electrical impedance spectroscopy (EIS) as a label free and noninvasive analysis method receives growing attention for monitoring three-dimensional tissue constructs. In this Article, we present the integration of an EIS readout function into the hanging-drop network platform, which has been designed for culturing microtissue spheroids in perfused multitissue configurations. Two pairs of microelectrodes have been implemented directly in the support of the hanging drops by using a small glass inlay inserted in the microfluidic structure. The pair of bigger electrodes is sensitive to the drop size and allows for drop size control over time. The pair of smaller electrodes is capable of monitoring, on the one hand, the size of microtissue spheroids to follow, for example, the growth of cancer microtissues, and, on the other hand, the beating of cardiac microtissues in situ. The presented results demonstrate the feasibility of an EIS readout within the framework of multifunctional hanging-drop networks.

[*]**Corresponding Author** olivier.frey@bsse.ethz.ch. Phone: +41 61 387 3344. Fax: +41 61 387 3994.
[†]Y.R.F.S. and S.C.B. contributed equally
[‡]Y.R.F.S.: ETH Zurich, Department of Biosystems Science and Engineering, Bioanalytics Group, Vladimir-Prelog-Weg 3, CH-8093 Zurich, Switzerland.

Author contributions

Notes
The authors declare no competing financial interest.

Europe PMC Funders Author Manuscripts
Europe PMC Funders Author Manuscripts

Europe PMC Funders Author Manuscripts

Europe PMC Funders Author Manuscripts

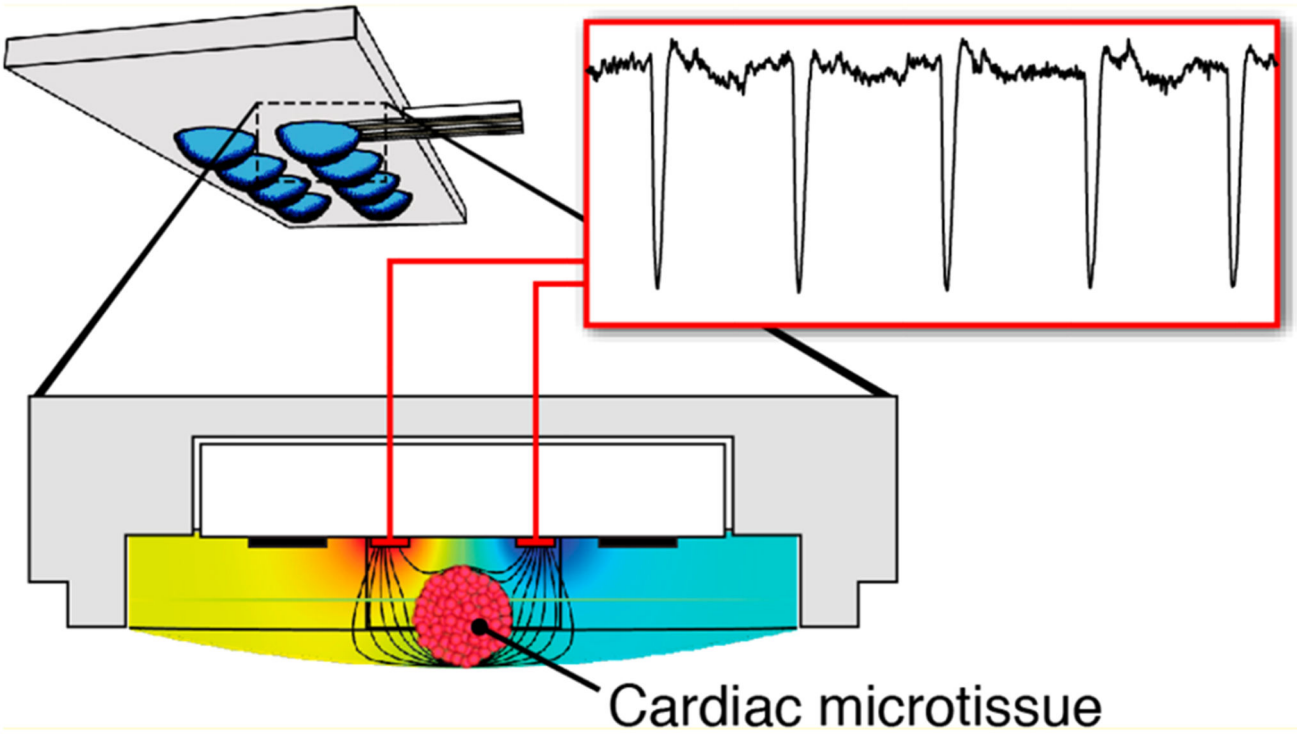

Keywords

microelectrode; impedance sensor; tumor growth; cardiac spheroid; body on a chip

Multicellular microtissue spheroids constitute an important in vitro tissue model system in pharmaceutical compound development and are used as simple organ models in basic research.[1–3] Their three-dimensional (3D) structure provides cells with a more in vivo like environment resulting in improved cell-specific functionality over longer periods of time compared to cells in two-dimensional cell cultures. Cell constructs that are able to approximately reproduce a humanbody response to pharmacological compounds are important for drug discovery and studying human physiology.[4] A central strength of microtissue spheroids compared to other engineered tissue formats is that they can be formed from several cell types giving access to many organ models based on the same tissue engineering technology.[5–10] Further, their compact morphology makes them relatively easy to handle on a larger scale by using many of the established cell culturing tools.

These advantages provide good reasons for their wide application in research and industry and the fact that more and more culturing systems and assays are specifically designed for use with spheroids. Among those are microfluidic assay setups. Capable of manipulating small amounts of liquid volumes and, at the same time, small amounts of biological material down to single cells,[11,12] microfluidic systems have also become an important tool for culturing spheroids and for precisely controlling the spheroid environment in space and time. Spheroids can be either loaded into microfluidic devices after off-chip formation[13–16]

Europe PMC Funders Author Manuscripts

Europe PMC Funders Author Manuscripts

or directly aggregated in the microfluidic chips.[17–23] Once properly positioned in such a microfluidic chip, they can be cultured and exposed to different compounds, while they can be analyzed through microscopy and biochemical assays. The small dimensions of the microfluidic networks and tissue structures allows for using several identical arrangements side-by-side, so that experiments can be executed in a parallelized fashion.

Despite these advancements in the past years, there is still a lack of methods for online monitoring or analysis of microtissues. Most of the current methods have been optimized for 2D cell layers and have to be made compatible with 3D tissue formats, or they have to be newly developed. Microscopy of tissue assemblies thicker than 200 μm, for example, suffers from low light penetration depths and light scattering, which limits its use for microtissue analysis.

Microfluidic culturing systems offer the possibility of directly integrating sensors close to the cellular assemblies by using microfabrication techniques. Electrical impedance spectroscopy (EIS), for example, receives growing attention and has previously been used for the analysis of various types of single cells.[24–26] EIS is based on applying an AC voltage to a set of microelectrodes and reading out the resulting current to calculate the corresponding interelectrode impedance values. Objects placed in the electric field between these electrodes characteristically modulate the impedance properties so that impedance spectroscopy can be used to assess samples located between the electrodes. EIS is label-free and noninvasive and can be integrated on a small scale, which allows for in situ assessment of cells and tissues.

Recently, different systems have been presented that prove the feasibility of EIS analysis for spheroids.[27] Apoptosis or tissue necrosis in breast carcinoma spheroids upon drug exposure has been analyzed by using a capillary screening system.[28] The handling of the capillary system was later improved by a chip featuring microwells with electrodes for EIS measurements located at the side walls.[29] Another spheroid EIS chip relied on high-aspect-ratio SU-8 structures within a PDMS channel to trap a spheroid between a set of facing and interdigitated electrodes.[30] It was shown that the EIS measurements could be used to discriminate different dilutions of the microtissue medium and various particle sizes.

Here, we present the integration of electrical impedance spectroscopy into the hanging-drop network platform.[22] Hanging-drop networks consist of an array of interconnected hanging drops that are specifically designed for spheroid aggregation and culturing. They allow for precise control of spheroid culturing conditions under flow and enable on-chip intertissue communication, which is at the base of realizing 3D microtissue body-on-a-chip configurations. The measuring electrodes have been integrated in a modular setup as small inlays and are located in the support structure of the hanging drops, in which then the spheroids of interest were cultured. The electrodes allowed for measuring the size of tumor spheroids and for monitoring the beating frequency of cardiac spheroids under continuous perfusion. Further, the size of the hanging drop itself could be read out, which is important for long-term operation of the hanging-drop network.

Europe PMC Funders Author Manuscripts

Europe PMC Funders Author Manuscripts

Experimental Section

Device Fabrication and Assembly

The hanging-drop network has been fabricated by using polydimethylsiloxane (PDMS) casting from a three-layer SU-8 mold. The electrode inlays were fabricated on glass and the electrodes were patterned by using lift-off technology. Both processes are well established and described in the Supporting Information including Figure S-1. The glass inlays were fixed and wire bonded onto a custom-made printed circuit board (PCB) that served as interface for the electric connections to the four electrodes. The glass inlay was inserted into the recess of the PDMS hanging-drop network and fixed by applying two-component glue between the PCB and the microscope slide to which the hanging-drop network was previously bonded. In some device assemblies, the glass inlay protruded the PDMS in a range of 50-100 μm, which, however, did not alter the functionality of the device. In all cases, the electrode plane has been chosen as origin for the drop height measurements. The device was fixed on a custom-made device holder, which was placed inside a polystyrene box together with a humidifier pad to reduce evaporation (see Figure S-2 for pictures of the fabricated devices).

Experimental Setup

For liquid control, we used high-precision syringe pumps and plastic or glass syringes with Luer-Lock connectors. The syringes were connected to rigid PTFE tubing. On the other end of the tubing, we used right-angled metal tips as connectors to the hanging-drop network.

The impedance setup comprised of an impedance spectroscope (HF2IS) and a transimpedance amplifier (HF2TA, both from Zurich Instruments AG, Switzerland). The transimpedance amplifier was interconnected between sensing electrodes and the input of the impedance spectroscope. The stimulating electrodes were directly connected to the output of the impedance spectroscope. We used shielded coaxial cables for all connections.

All experiments were carried out on a Leica DMI6000B inverted microscope, placed inside an environmental chamber featuring a controlled temperature of 37 °C. We used a Leica DFC 340FX CCD camera for image acquisition. The heights of the hanging drops were measured by using the z-position of the microscope objective and setting the focal plate to the lowest point of the drops.

Liquid Handling

The HDN was continuously perfused with spheroid-specific maintenance medium (see section *Cell culturing* in the Supporting Information) while performing the EIS recordings. The inflow and outflow rates were kept at 10 μL/min unless otherwise noted. Since the HDN comprised two parallel rows of drops (cf. Figure 1A), the effective flow rate through each row was 5 μL/min. For the same inflow and outflow rates, the drop sizes remained constant. The drop size could be increased or decreased by increasing the inflow or outflow rate to 20 μL/min while keeping the other flow rate at 10 μL/min. EIS recordings did not start earlier than 10 s after changing the flow rates, to allow for drop size and EIS signal stabilization.

Europe PMC Funders Author Manuscripts

Europe PMC Funders Author Manuscripts

Initial liquid loading was carried out after having applied an oxygen plasma treatment to selectively increase the wettability of the PDMS inside the drop structures. Liquid medium was applied by using a standard pipet.

The spheroids were loaded into the chip by flipping the chip upside down and letting the spheroid sediment from a pipet into the drop, which was facing upward. After loading a spheroid the chip was flipped back and the liquid network was perfused with fresh medium for at least 1 min to reduce the influence of liquid carry-over from the spheroid culturing plate.

Impedance Measurements

The EIS recordings were performed by means of an HF2IS impedance spectroscope that generated the input voltage of the chip and recorded the resulting output current signal. Measurement data were stored on a PC for later off-line analysis using a custom MATLAB tool. The impedance spectra were recorded in two different modes: (i) continuous frequency sweeping for measuring spheroid and drop sizes and (ii) using eight specific frequencies in parallel for the characterization of the cardiac beating behavior and spheroid growth. For the sweeps, the frequency was increased from 100 Hz to 40 MHz in equidistant steps on a logarithmic scale. For the parallel assessment, eight frequencies were chosen equidistantly on a logarithmic scale between 10 kHz and 15 MHz and superimposed via the same electrode set. In both cases, the output voltage amplitude was set to 100 mV per frequency. The resulting current recorded from the chip was transformed into a voltage by using an off-chip HF2TA transimpedance amplifier at a feedback gain of 100 V/A. The experimentally obtained output signals are, therefore, displayed in units of "volts" in the figures, which represent a direct measure of the impedance. For the sweeps, raw signal magnitude values are displayed.

Simulations

Three-dimensional simulations of the impedance in a hanging drop were conducted by using COMSOL 4.3a (COMSOL Multiphysics GmbH, Germany). The drop was approximated as a spherical cap attached to a cylinder, both with base diameter of 3.5 mm. The conductivity of the medium was set to 1.2 S/m approximating that of RPMI 1640 growth medium. An electrical current study was performed by applying a voltage of 1 V across the respective electrodes. The spheroid was approximated by a non-conductive sphere, introduced at the bottom of the drop.

Results and Discussion

Design of the Microfluidic Device

Previously, we demonstrated that it is possible to array hanging drops in an open microfluidic system by constraining the fluid spreading by an arrangement of hydrophilic and hydrophobic PDMS surfaces and rims so that parallel multitissue interaction studies could be performed.[22] The device presented here relies on the same approach so that all previously developed functions of the hanging-drop network (HDN) technology are preserved. The integration of electrodes and impedance spectroscopy functionality into the

Europe PMC Funders Author Manuscripts

Europe PMC Funders Author Manuscripts

hanging-drop network was realized by using a modular, hybrid approach. The idea was to fabricate the electrodes on a small glass inlay by using standard MEMS fabrication methods. The inlay then fits into a recess in the microfluidic hanging-drop device. Figure 1A shows the microfluidic layout of the device consisting of two rows of four drops with a single inlet and a single outlet. The liquid is confined by PDMS rims surrounding the drops and microchannels. We further included two loading ports for additional fluid connections. The rectangular recess for the glass inlay was implemented at the location of one of the drops. As can be seen, the recess also interrupts the rim structure. Therefore, an SU-8 rim structure on the inlay itself (indicated in green color) is used to complete the rim once the inlay has been placed in the recess so that the fluidic confinement of the device is preserved. Plugging the inlay into the PDMS device is schematically illustrated in Figure 1B. The modular approach is not limited to the current design, but allows for individual adaptations of the microfluidic layout, the electrode configuration on the inlay, and the number of inserted inlays so that more complex multifunctional hanging-drop networks can be realized.

Figure 1C shows the design of the inserted inlay in details featuring two pairs of Pt electrodes located around the center of the drop. The SU-8 walls on the inlay complement the PDMS rim. We designed big electrodes near the edges of the inlay to measure the size of the hanging drop. We also fabricated a pair of smaller electrodes to measure the impedance near the center of the drop. The smaller electrodes are used to assess the size of microtissue spheroids and to record the beating of cardiac spheroids. As hanging drops can be varied in size, the drop height has been reduced and thereby the spheroid has been moved upward closer to the electrodes in order to increase impedance measurement sensitivity. Additional SU-8 structures form a trap so that the spheroids are reliably positioned between the electrodes upon reduction of the drop size. Further, these SU-8 structures also help to focus the electric field between the small electrodes. Figure 1D shows a crosssection through the drop indicating dimensions and illustrating the position of the electrodes at the drop ceiling. Pictures ofthe fabricated devices can be found in Figure S-2.

Measuring Drop Heights through EIS

Drop sizes in a microfluidic hanging-drop network can vary upon changing flow protocols, so that, in contrast to closed microfluidic systems, the volume in such open microfluidic systems also can change. A higher inflow rate, compared to the outflow rate, for example, leads to an increase in drop size and can make drops drip off in the most unfavorable case. A possibility to continuously measure the drop size—preferably independently of a microscope–is, therefore, highly desirable.

We used the big electrodes at the edge of the glass inlay for drop size monitoring. The electrical field generated between the two electrodes is confined through the conducting liquid (Figure 2A). As a function of the drop volume and height, the electric field lines are either compressed or expanded, which changes the impedance between the electrodes. Position and size of the electrodes have been optimized with respect to maximal sensitivity to drop size by using numerical simulations with COMSOL software (Figure S-3). As a result, electrodes were placed at maximum distance within the drop radius and were made as wide as possible within the geometrical margins of the inlay.

Europe PMC Funders Author Manuscripts

Europe PMC Funders Author Manuscripts

We observed a significant dependence of the signal magnitude on drop height and medium conductivity over a large spectrum of frequencies. An important parameter in the system included liquid or water evaporation from the drops. Evaporation not only led to a reduction of the drop size, but also to an increase in medium salinity and conductivity. These two effects influenced the recorded signals and resulted in low baseline stability and considerable signal drift (Figure S-4). To counteract these effects, we conducted the measurements under continuous-flow conditions at a flow rate larger than 5 μL/min, so that no baseline drift was observed. It is worth mentioning that, compared to the setup here, biological experiments are generally conducted at similar flow rates, however, at much higher relative humidity levels in incubators (>90% as opposed to 40—50% here), which substantially reduces evaporation.

A clear change in the spectra has been measured as a function of the drop height (600—1300 μm), as is depicted in Figure 2B. The largest difference between the signal magnitude curves and, hence, highest sensitivity to drop size was observed at 730 kHz (dotted line, see also differential magnitude in Figure S-5). At the same time, the magnitude spectra recorded at the beginning and at the end of an experiment (~4 h overall experiment duration) were very similar (see zoomed view of the two curves at 1300 μm drop height in Figure 2B). The impedance measurement was, therefore, reproducible over time and showed only a minor drift. The dependence of the signal magnitude at 730 kHz upon drop height is plotted in Figure 2C (big electrodes, circles). We observed that the signals of the small electrodes (originally designed for spheroid detection) also showed some drop-height dependence, but were significantly less sensitive to drop height, especially for larger drops (Figure 2C, crosses). This effect can be assigned to comparably smaller changes in the electric field between the small electrodes upon drop height variation.

These drop-size calibration measurements were performed without the presence of a spheroid in the hanging drops. The presence of a spheroid, however, influenced the signals obtained by the big electrodes as well, especially when the drop height was small (~700 μm). Consequently, some interference between drop size measurements and presence of a microtissue exists, which is, however, relatively small (see Figure S-6). The normal culturing conditions involve large drop heights (1300 μm), which then have to be controlled by impedance measurements. For these large drop heights, the impedance signal of the big electrode set was found to be largely independent of the presence of a spheroid.

Measuring Spheroid Size through EIS

The small electrodes were placed close to the presumable spheroid location, but off-center in order to allow for optical access to the spheroid. For measuring the spheroid size, the drop size has been reduced in a controlled way so that the spheroid located at the liquid-air interface at the bottom center of the drop was lifted upward to a location between the electrodes and inside the electrical field. By applying this strategy, the presence of the spheroid disturbed the electric field lines and, consequently, changed the impedance much more than it would have been the case without reducing the drop size. The alteration of the electric field has been confirmed through simulations as shown in Figures 3AB. Here, output current values have been calculated as a result of impedance changes for an applied voltage

Europe PMC Funders Author Manuscripts

Europe PMC Funders Author Manuscripts

of 1 V. The changes in current magnitudes in dependence of the spheroid size were found to be the larger, the shorter the spheroid-electrode distance was.

Figure 3C shows photographs of a hanging drop of colored liquid of two different heights below the recording electrodes (no spheroid was present for these pictures). SU-8 trapping structures were used to precisely position the spheroid between the electrodes when decreasing the height of the hanging drop. Figure 3D shows micrographs of two spheroids of different sizes positioned in the SU-8 trap for a drop height of 600 μm. Further, the SU-8 structures help to confine the electrical field lines, thereby improving sensitivity.

We measured a clear frequency-dependent impedance magnitude change in dependence of the spheroid size. Figure 3E presents the impedance spectra of two different spheroid sizes (400 and 600 μm in diameter) recorded for a drop height of 600 μm, and two spectra of the empty drop. The spectra are clearly separated. The impedance change in dependence of the spheroid size was visible at different drop heights (600, 700, and 900 μm) and decreased with increasing drop height (Figure S-7A-C). This trend is even more pronounced in Figure S-7D-F showing *the signal magnitude differences*, calculated as the signal magnitude of a drop containing a spheroid of a certain size after subtraction of the impedance magnitude of the respective empty drop. The magnitudes of empty drops were again measured at the beginning and at the end of the experiments. The variation of the magnitude values between these two time points is low for all drop heights, (Figure 3E and S-7G-I), which proves the robustness of EIS measurements over time under flow conditions. This variation can be taken as a measure of the signal stability and baseline drift of the system. In a next step, we tried to establish a relation between *spheroid-size-induced changes in the impedance magnitude and the f luctuation over time of the empty-drop impedance signal*. It is evident that drop size variations, baseline drift and their influence on the impedance signals have to be kept at a minimum in order to enable reliable spheroid-size measurements, which entails that the flow rate through the hangingdrop system must be precisely controlled. The ratio of *spheroid size-induced signal changes to f luctuation in the empty-drop signal*, thus, will give a measure of how repeatable the microtissue size measurements are over time. Figure 3F shows a plot of this ratio for the two different spheroid sizes and three different drop heights over the full impedance frequency range. As can be seen, there are different optimal frequencies for the various drop heights. Further, as expected, the largest values were observed for small drop heights (z = 600 μm). In this particular case, the signal change due to baseline fluctuations over time is in the range of 0.5% of the signal difference between a spheroid with a diameter of 400 μm and a spheroid of 600 μm. This results in a diameter resolution of below 5 μm in that specific size range considering three times the baseline drift as limit for the minimal detectable signal. The optimal frequency was in all cases only depending on the drop height and was the same for both spheroid sizes. It should be noted that Figure 3F has a log scale on the *y*-axis. Figure 3G presents the signal magnitudes at the optimal frequencies per drop height and for different spheroid sizes (a spheroid size of 0 μm represents the value of the empty drop). The trends in the measured values qualitatively resemble those of the simulation (Figure 3B). Finally, Figure 3H presents the system sensitivities ($\mu V/\mu$m) for measuring spheroid sizes in hanging drops of different drop heights. They were calculated as signal magnitude change at optimal frequency (in μV) per variation in spheroid diameter (in μm). The left bars in each group

represent the output signal sensitivity in $\mu V/\mu m$ for the range between no spheroid present until 400 μm spheroid diameter, while the right bars represent the output signal sensitivity in $\mu V/\mu m$ for the diameter range between 400 and 600 μm. Again, the highest sensitivity was obtained for small drop heights (600 μm), at which the spheroid is positioned close to the electrodes. Further, the sensitivity with respect to diameter changes above 400 μmis higher. For the current spheroid trap, only spheroids smaller than ~700 μm can be measured. Larger spheroids would not fit in between the SU-8 trap structures (see Figure 3D).

We further investigated the possibility of continuously monitoring spheroid growth over time. Gravity-induced spheroid aggregation requires hanging drops with a large curvature ($z > 1200$ μm). Once the spheroid has been formed, the drop height can be permanently reduced to 600 μm for subsequent EIS measurements (Figure 3I). Figure 3J shows the continuous decrease of the signal magnitudes of -22-26% at different frequencies over 40 h as a result of a growing HCT116 colon cancer spheroid (images in Figure 3I). Nongrowing human liver spheroids produced the expected constant signal magnitudes with a decrease of <0.5% over 13 h. In control experiments without spheroids in the hanging drops, signal magnitudes varied less than 0.5% over time for frequencies between 192 kHz and 1 MHz (Figure S-8).

Detection of Cardiac Microtissue Contractions through EIS

The spontaneous beating of cardiac spheroids (hCdMT) was assessed by using multifrequency EIS and microscope video recording in parallel. For these measurements, the drop height was again reduced, so that the hCdMT was positioned inside the SU-8 trap between the small electrode pair. Figure 4A shows the baseline-subtracted 5.3 MHz magnitude signal (red, right axis) and the differential and thresholded pixel count of the video sequence (blue, left axis), which were acquired in parallel. The signal magnitude at a frequency of 5.3 MHz was found to yield the highest signal-to noise ratio. The spikes in the EIS signal coincided with spikes in the optical signal and corresponded to contractions of the cardiac tissue. The change in the impedance signal upon beating of the tissue was due to changes in shape and geometry of the spheroid. The spheroid was located between the electrodes and, therefore, any shape change upon contraction of the spheroid altered the interelectrode impedance. The changes in the optical signal upon deformation of the tissue showed a double peak for every contraction owing to the differential image analysis. The optical signal was extracted as the (absolute) difference of succeeding video frames, after thresholding and estimating the number of pixel changes above threshold. The correlation between the impedance signal and optical recordings shows that EIS is a suitable method to extract the beating rate of a cardiac spheroid in a hanging drop. The details of the beating analysis are shown for a single contraction-relaxation cycle in Figure 4B: The differential image sequence was obtained by subtracting the first frame from all following frames in the video sequence. Thus, dark pixels constitute changed pixels and white pixels correspond to unchanged pixels in reference to the first image frame. From the sequence it can be seen that,in agreement with previous reports,[7] the contraction of the microtissue spheroid was happening in less than 200 ms, whereas the relaxation was taking up to 1 s. The same outcome can be observed in the multifrequency magnitude spectra shown in Figure 4C that have been recorded at the same time points as the video frames depicted in Figure 4B.

Europe PMC Funders Author Manuscripts
Europe PMC Funders Author Manuscripts

Europe PMC Funders Author Manuscripts

Europe PMC Funders Author Manuscripts

Conclusions

We present a new method for the analysis of microtissue spheroids relying on electrical impedance spectroscopy inside a hanging drop. We have used a modular approach by realizing glass inlays carrying the electrodes for the hanging-drop microfluidic systems. These glass inlays were placed into recesses of the microfluidic drop support, so that the electrodes are placed in the “ceilings”. The modularity of this approach allows for great flexibility in designing hanging-drop networks and for selecting the hanging drops, in which the EIS functionality should be added for in situ monitoring. Further, the technological approach of the presented electrode integration into hanging-drop networks can be used for a variety of other sensor types including, for example, biosensors. The overall microfluidic layout, based on PDMS, remains the same, so that all previously developed functions of the hangingdrop network technology are preserved.

The system has been optimized with respect to electrode dimensions, spheroid positioning, definition of the electric field and performance of the experimental setup. We further developed methods for evaluating measurement frequencies to obtain maximal sensitivity and stability over time. These methods are required to deal with chip-to-chip variations and the influence of external effects originating from the fact that impedance spectroscopy is a very sensitive method. In proof-of-concept studies we measured the different sizes of cancer spheroids by using EIS. Further, the beating of cardiac spheroids could be recorded in real-time directly inside the hanging drop and could be correlated to the results of optical imaging. We demonstrated that EIS is suited to monitor and control experimental parameters, such as the height of hanging drops, so that automated drop height control and adjustment is feasible. Finally, the growth of cancer spheroids could be continuously monitored over 2 days by means of EIS in a perfused on-chip culture.

With the presented EIS integration we realized an important new readout feature for the hanging-drop network platform, which is independent of and complementary to optical observation through a microscope and has the potential to record at higher temporal resolution as a feature for future applications.[24,26] The method will enable us to acquire comprehensive data sets in multitissue or so-called “body-on-a-chip” experiments.

Associated Content

Refer to Web version on PubMed Central for supplementary material.

Acknowledgments

This work was financially supported by FP7 of the EU through the projects “Body on a chip”, ICT-FET- 296257 and the ERC Advanced Grant “NeuroCMOS” (Contract 267351), as well as by an individual Ambizione Grant 142440 of the Swiss National Science Foundation for O.F. We would like to thank InSphero AG, Schlieren, Switzerland, for providing cardiac microtissues and related culture medium. We further thank Alexander Stettler of the BSSE Cleanroom Facility for support with the microfabrication.

References

(1). Hirschhaeuser F, Menne H, Dittfeld C, West J, Mueller-Klieser W, Kunz-Schughart La. Multicellular Tumor Spheroids: An Underestimated Tool Is Catching up Again. J Biotechnol. 2010; 148: 3–15. [PubMed: 20097238]

Europe PMC Funders Author Manuscripts

Europe PMC Funders Author Manuscripts

(2). Kunz-Schughart, La. The Use of 3-D Cultures for High-Throughput Screening: The Multicellular Spheroid Model. J Biomol Screening. 2004; 9: 273–285.

(3). Fennema E, Rivron N, Rouwkema J, van Blitterswijk C, de Boer J. Spheroid Culture as a Tool for Creating 3D Complex Tissues. Trends Biotechnol. 2013; 31: 108–115. [PubMed: 23336996]

(4). Griffith LG, Swartz Ma. Capturing Complex 3D Tissue Physiology in Vitro. Nat Rev Mol Cell Biol. 2006; 7: 211–224. [PubMed: 16496023]

(5). Kelm JM, Fussenegger M. Microscale Tissue Engineering Using Gravity-Enforced Cell Assembly. Trends Biotechnol. 2004; 22: 195–202. [PubMed: 15038925]

(6). Drewitz M, Helbling M, Fried N, Bieri M, Moritz W, Lichtenberg J, Kelm JM. Towards Automated Production and Drug Sensitivity Testing Using Scaffold-Free Spherical Tumor Microtissues. Biotechnol J. 2011; 6: 1488–1496. [PubMed: 22102438]

(7). Beauchamp P, Moritz W, Kelm JM, Ullrich ND, Agarkova I, Anson BD, Suter TM, Zuppinger C. Development and Characterization of a Scaffold-Free 3D Spheroid Model of Induced Pluripotent Stem Cell-Derived Human Cardiomyocytes. Tissue Eng Part C. 2015; 21: 852–861.

(8). Rimann M, Laternser S, Gvozdenovic A, Muff R, Fuchs B, Kelm JM, Graf-Hausner U. An in Vitro Osteosarcoma 3D Microtissue Model for Drug Development. J Biotechnol. 2014; 189: 129–135. [PubMed: 25234575]

(9). Zuellig, Ra; Cavallari, G; Gerber, P; Tschopp, O; Spinas, Ga; Moritz, W; Lehmann, R. Improved Physiological Properties of Gravity-Enforced Reassembled Rat and Human Pancreatic PseudoIslets. J Tissue Eng Regener Med. 2014; doi: 10.1002/term.1891

(10). Urich E, Patsch C, Aigner S, Graf M, Iacone R, Freskgard P-O. Multicellular Self-Assembled Spheroidal Model of the Blood Brain Barrier. Sci Rep. 2013; 3

(11). Dittrich PS, Manz A. Lab-on-a-Chip: Microfluidics in Drug Discovery. Nat Rev Drug Discovery. 2006; 5: 210–218. [PubMed: 16518374]

(12). El-Ali J, Sorger PK, Jensen KF. Cells on Chips. Nature. 2006; 442: 403–411. [PubMed: 16871208]

(13). Ruppen J, Cortes-Dericks L, Marconi E, Karoubi G, Schmid Ra, Peng R, Marti TM, Guenat OT. A Microfluidic Platform for Chemoresistive Testing of Multicellular Pleural Cancer Spheroids. Lab Chip. 2014; 14: 1198–1205. [PubMed: 24496222]

(14). Kim J-Y, Fluri Da, Marchan R, Boonen K, Mohanty S, Singh P, Hammad S, Landuyt B, Hengstler JG, Kelm JM, et al. 3D Spherical Microtissues and Microfluidic Technology for MultiTissue Experiments and Analysis. J Biotechnol. 2015; 205: 24–35. [PubMed: 25592049]

(15). Kim J-Y, Fluri Da, Kelm JM, Hierlemann A, Frey O. 96-Well Format-Based Microfluidic Platform for Parallel Interconnection of Multiple Multicellular Spheroids. J Lab Autom. 2015; 20: 274–282. [PubMed: 25524491]

(16). Das T, Meunier L, Barbe L, Provencher D, Guenat O, Gervais T, Mes-Masson A-M. Empirical Chemosensitivity Testing in a Spheroid Model of Ovarian Cancer Using a Microfluidics-Based Multiplex Platform. Biomicrofluidics. 2013; 7 011805

(17). Hsiao AY, Torisawa Y, Tung Y-C, Sud S, Taichman RS, Pienta KJ, Takayama S. Microfluidic System for Formation of PC-3 Prostate Cancer Co-Culture Spheroids. Biomaterials. 2009; 30: 3020–3027. [PubMed: 19304321]

(18). Torisawa Y, Takagi A, Nashimoto Y, Yasukawa T, Shiku H, Matsue T. A Multicellular Spheroid Array to Realize Spheroid Formation, Culture, and Viability Assay on a Chip. Biomaterials. 2007; 28: 559–566. [PubMed: 16989897]

(19). Kim T, Doh I, Cho Y-H. On-Chip Three-Dimensional Tumor Spheroid Formation and Pump-Less Perfusion Culture Using Gravity-Driven Cell Aggregation and Balanced Droplet Dispensing. Biomicrofluidics. 2012; 6 034107

(20). Ruppen J, Cortes-Dericks L, Marconi E, Karoubi G, Schmid Ra, Peng R, Marti TM, Guenat OT. A Microfluidic Platform for Chemoresistive Testing of Multicellular Pleural Cancer Spheroids. Lab Chip. 2014; 14: 1198–1205. [PubMed: 24496222]

(21). Wu LY, Di Carlo D, Lee LP. Microfluidic Self-Assembly of Tumor Spheroids for Anticancer Drug Discovery. Biomed Microdevices. 2008; 10: 197–202. [PubMed: 17965938]

(22). Frey O, Misun PM, Fluri Da, Hengstler JG, Hierlemann A. Reconfigurable Microfluidic Hanging Drop Network for Multi-Tissue Interaction and Analysis. Nat Commun. 2014; 5

Europe PMC Funders Author Manuscripts

(23). Kwapiszewska K, Michalczuk A, Rybka M, Kwapiszewski R, Brzozka Z. A Microfluidic-Based Platform for Tumour Spheroid Culture, Monitoring and Drug Screening. Lab Chip. 2014; 14: 2096–2104. [PubMed: 24800721]

(24). Haandbæk N, Burgel SC, Heer F, Hierlemann A. Characterization of Subcellular Morphology of Single Yeast Cells Using High Frequency Microfluidic Impedance Cytometer. Lab Chip. 2014; 14: 369–377. [PubMed: 24264643]

(25). Zhu Z, Frey O, Ottoz DS, Rudolf F, Hierlemann A. Microfluidic Single-Cell Cultivation Chip with Controllable Immobilization and Selective Release of Yeast Cells. Lab Chip. 2012; 12: 906–915. [PubMed: 22193373]

(26). Holmes D, Pettigrew D, Reccius CH, Gwyer JD, van Berkel C, Holloway J, Davies DE, Morgan H. Leukocyte Analysis and Differentiation Using High Speed Microfluidic Single Cell Impedance Cytometry. Lab Chip. 2009; 9: 2881. [PubMed: 19789739]

(27). Alexander, Fa; Price, DT; Bhansali, S. From Cellular Cultures to Cellular Spheroids: Is Impedance Spectroscopy a Viable Tool for Monitoring Multicellular Spheroid (MCS) Drug Models? IEEE Rev Biomed Eng. 2013; 6: 63–76. [PubMed: 23335673]

(28). Thielecke H, Mack A, Robitzki A. A Multicellular Spheroid-Based Sensor for Anti-Cancer Therapeutics. Biosens Bioelectron. 2001; 16: 261–269. [PubMed: 11390213]

(29). Kloss D, Kurz R, Jahnke H-G, Fischer M, Rothermel A, Anderegg U, Simon JC, Robitzki Aa. Microcavity Array (MCA)-Based Biosensor Chip for Functional Drug Screening of 3D Tissue Models. Biosens Bioelectron. 2008; 23: 1473–1480. [PubMed: 18289841]

(30). Luongo K, Holton A, Kaushik A, Spence P, Ng B, Deschenes R, Sundaram S, Bhansali S. Microfluidic Device for Trapping and Monitoring Three Dimensional Multicell Spheroids Using Electrical Impedance Spectroscopy. Biomicrofluidics. 2013; 7 034108

Europe PMC Funders Author Manuscripts

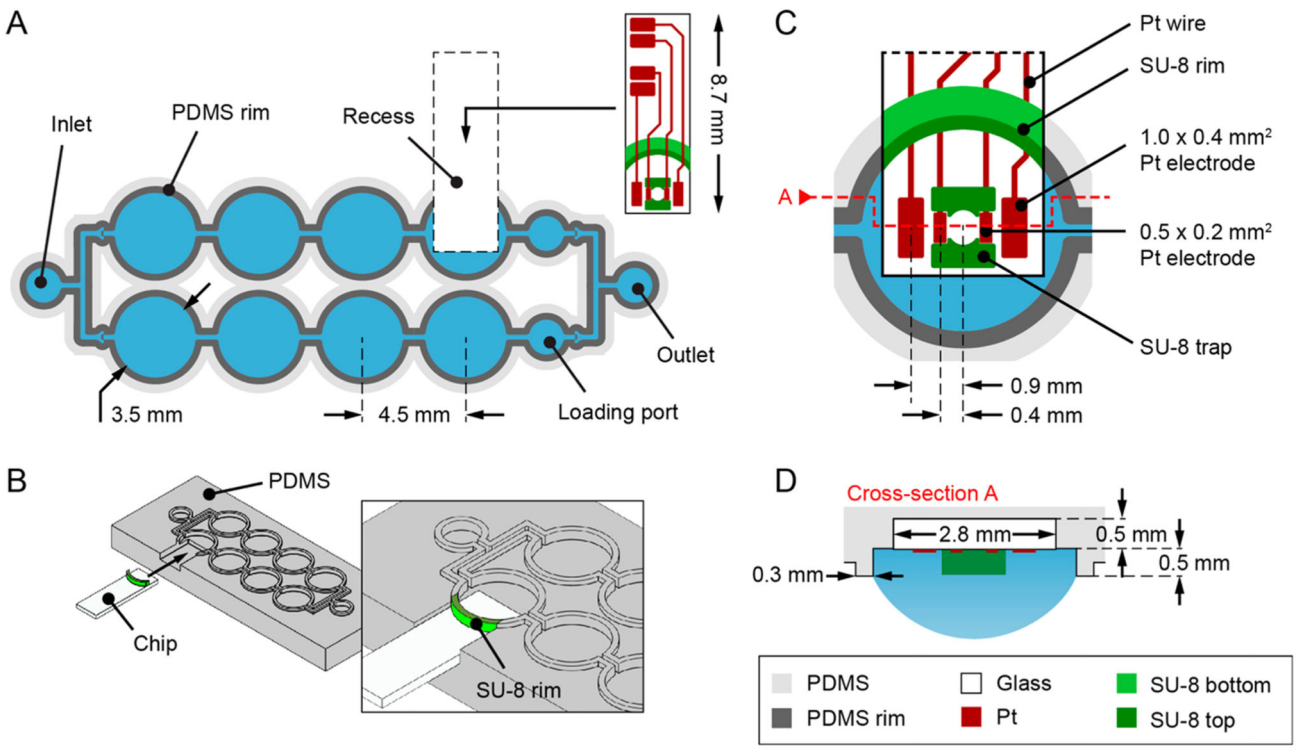

Figure 1. Design and concept of EIS-electrode integration in hanging-drop networks (HDNs).

(A) Overview of the 2 × 4 drop microfl uidic device and the glass inlay containing four electrodes. (B) 3D visualization illustrating the insertion and final placement (zoomed view) of the glass inlay into the PDMS device. (C) Detailed view of the glass inlay inserted into the hanging drop. SU-8 rim structures on the glass inlay complete the PDMS rim that confi nes the fluid. (D) Cross section of the hanging drop formed between the rim structures. The glass inlay is plugged into a recess in the PDMS so that the electrodes are located at the ceiling of the readout drop.

Europe PMC Funders Author Manuscripts
Europe PMC Funders Author Manuscripts

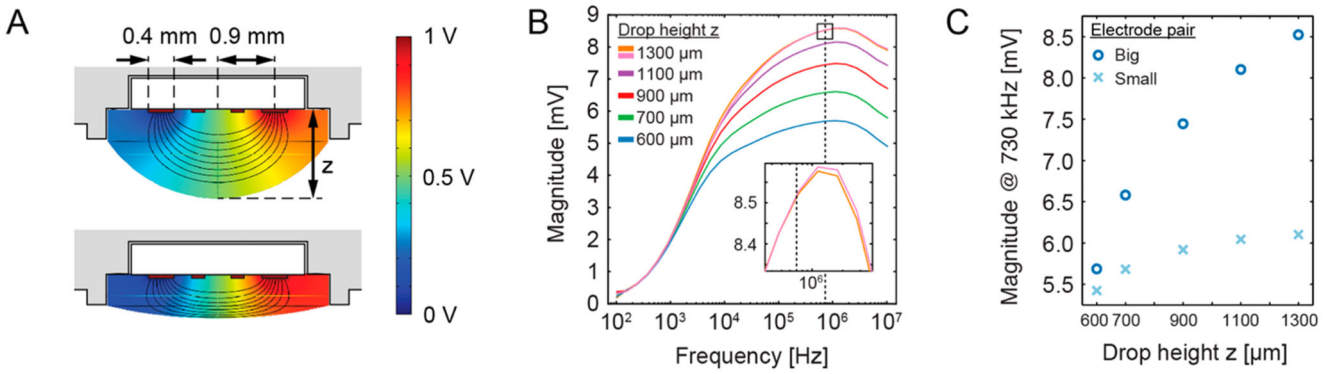

Figure 2. Hanging-drop height monitoring by using EIS.

(A) Simulation of the electric field lines in the hanging drop at two different drop heights. (B) Absolute signal spectra for different drop heights, which were recorded by using the big electrode pair. For z = 1300 μm the spectrum has been recorded before and after the measurements and showed only little variation (zoomed view in the inset). Dashed lines indicate the optimal frequency of 730 kHz. (C) Signal magnitude at 730 kHz for different drop heights as recorded with the big and small electrode pairs.

Europe PMC Funders Author Manuscripts

Europe PMC Funders Author Manuscripts

Europe PMC Funders Author Manuscripts

Europe PMC Funders Author Manuscripts

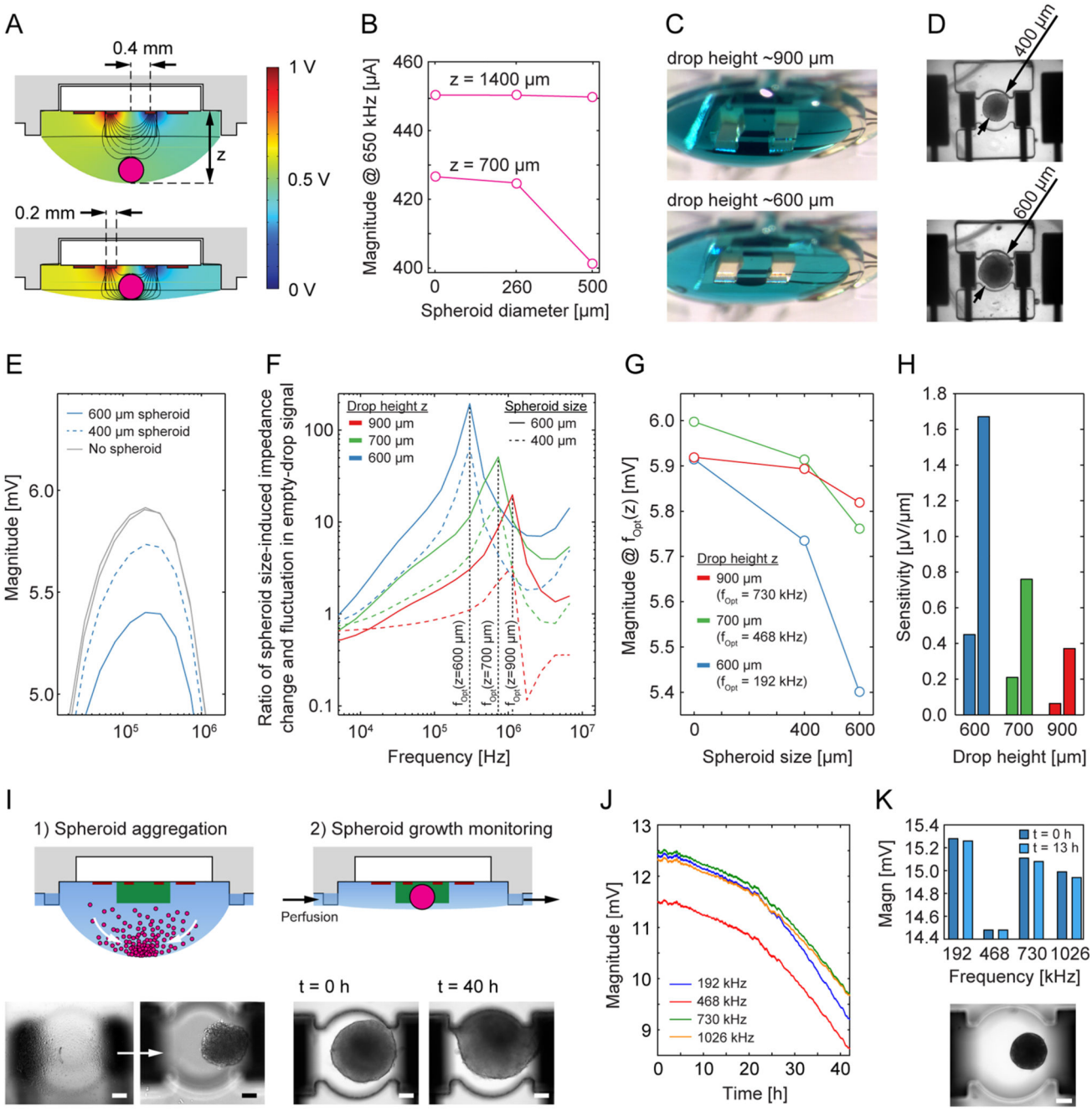

Figure 3. Spheroid size measurements through EIS.

(A) Modeling of the tissue-evoked impedance changes in hanging drops for two different drop heights (700 and 1400 μm). (B) Based on the model, the current signals of two different spheroid sizes (260 and 500 μm) have been simulated for a applied voltage of 1 V. Low drop heights entail higher signal sensitivity to spheroid size. The 0-μm value corresponds to that of an empty drop with no spheroid present. (C) Photographs of hanging drops of colored liquid of different heights below the recording electrodes (no spheroid was present for these pictures). (D) Micrographs of two spheroids (400 and 600 μm diameter)

positioned in the SU-8 trap in the drop support. (E) Signal magnitude spectra as a function of spheroid size for two different spheroid diameters (400 and 600 μm) and the empty drop before and after the experiment. (F) Ratio of spheroid size-induced signal magnitude changes (spheroid diameters of 400 and 600 μm) and fluctuation in the empty- drop signal over the full frequency spectrum (log scale). Optimal frequencies for each drop height are indicated as dotted vertical lines. (G) Signal magnitudes of spheroids of different size at optimal frequencies for the different drop heights. The 0 μm value corresponds to that of an empty drop with no spheroid present. (H) Calculated sensitivities; the left bars in each group represent the output signal sensitivity in $\mu V/\mu$m for the range between no spheroid present until 400 μm spheroid diameter, while the right bars represent the output signal sensitivity in $\mu V/\mu$m for the diameter range between 400 and 600 μm. Measured signal magnitudes are raw measured values in units of volts (in contrast to the FEM model, where we had current values) due to the trans-impedance amplification. (I) Schematic of on-chip spheroid formation in the hanging drop and subsequent growth monitoring in low-height hanging drops including images at different time points (scale bars are 100 μm). (J) Signal magnitude over time of a growing HCT116 spheroid depicted in (I). (K) Signal magnitude variation of a nongrowing primary liver spheroid over 13 h (scale bar is 100 μm).

Europe PMC Funders Author Manuscripts

Europe PMC Funders Author Manuscripts

Europe PMC Funders Author Manuscripts

Europe PMC Funders Author Manuscripts

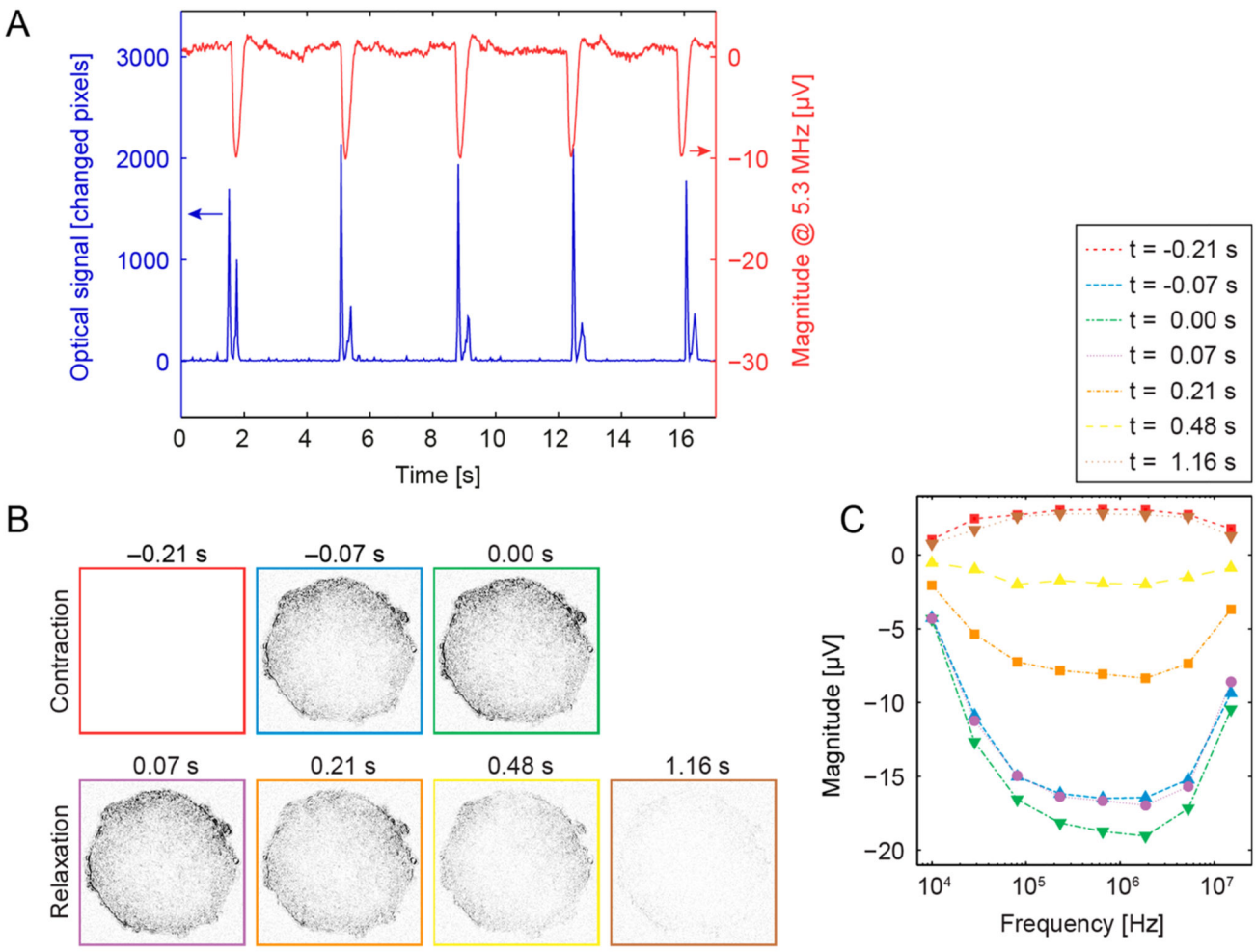

Figure 4. Monitoring of the contractions of human cardiac microtissue spheroids (hCdMT) in hanging drops.

(A) Beating sequences obtained by microscope video recordings (blue, left *y*-axis) and EIS-recordings (red, right *y*-axis). Single beat characteristics observed optically (B) in terms of differential images (first image frame is subtracted from the subsequent ones) and through EIS (C) in terms of signal magnitude spectra after baseline subtraction. The timing of the video frame acquisition coincided with selected time points in the impedance magnitude spectra. The time points are listed above the images in (B), in the legend in (C) and are indicated by color coding.